10.1002/ange.201914119

WILEY-VCH

RESEARCH ARTICLE

Low-fouling Fluoropolymers for Bioconjugation and In Vivo Tracking

Changkui Fu,[a] Baris Demir,[b] Sheilajen Alcantara,[c] Vinod Kumar,[d] Felicity Han,[d] Hannah G. Kelly,[c] Xiao Tan, [a] Ye Yu,[a] Weizhi Xu,[d] Jiacheng Zhao,[a] Cheng Zhang,[a] Hui Peng,[a] Cyrille Boyer,[e] Trent M. Woodruff,[d] Stephen J. Kent,[c] Debra J. Searles,[b] Andrew K. Whittaker*[a]

Abstract: The conjugation of hydrophilic low-fouling polymers to therapeutic molecules and particles is an effective approach to improving their aqueous stability and solubility, and extending their pharmacokinetics. Recent concerns over the immunogenicity of poly(ethylene glycol) has highlighted the importance of identifying alternative low fouling polymers. Herein, we report a new class of synthetic water-soluble homo-fluoropolymers with a sulfoxide side-chain structure. The incorporation of fluorine enables direct imaging of the homopolymer by ^{19}F MRI, negating the need for additional synthetic steps to attach an imaging moiety. These self-reporting fluoropolymers show outstanding imaging sensitivity and as such represent a new class of low-fouling polymer for bioconjugation and *in vivo* tracking.

Introduction

It is widely appreciated that decoration of therapeutic molecules with low-fouling polymers can dramatically improve their bioavailability in the form of increased stability, solubility and pharmacokinetics. A range of polymers have been used for this purpose and have facilitated the development of advanced (nano)medicines for more precise and effective treatment of diseases.[1] With all of these molecular and nanoparticles entities, it is important to be able to measure, in a facile manner, the *in vivo* location and concentration of the polymer-conjugated therapeutics after administration. Such information is closely related to the therapeutic outcome. Typically, this can be achieved by additionally conjugating imaging moieties such as fluorophores,[2] paramagnetic contrast agents (CAs),[3] or radioactive isotopes.[4] However, the additional chemical steps increase synthetic complexity; questions over the stability of the conjugation chemistry and the effect of the conjugated moiety on biological fate have been raised.[5] It therefore follows that there is an evident need and interest in developing self-trackable polymers for use in bioconjugation. Such self-trackable polymers remove the need for reaction with additional imaging moieties and inherently provide a measurable signal in the commonly-used imaging modalities to allow quantitative tracking of the polymer-conjugated therapeutics.[6]

^{19}F MRI is a powerful non-invasive imaging technique that has numerous applications in pre-clinical biomedical research, and potentially in the diagnosis and monitoring of human diseases.[7] A variety of fluorinated molecules and nanoparticles have been developed as ^{19}F MRI CAs.[8] Fluorine-containing polymers, namely fluoropolymers, are particularly attractive as macromolecular CAs due to their tunable size, structure and functionality, leading to improved pharmacokinetics, image contrast and resolution in comparison with small molecule CAs.[9] The use of fluoropolymers for bioconjugation is therefore a promising approach to enable the observation of the location and concentration of therapeutic conjugates by ^{19}F MRI. However, an obstacle to the widespread use of fluoropolymers for bioconjugation is the lack of aqueous-soluble fluoropolymers with sufficiently-high imaging sensitivity. The inherent hydrophobicity of the fluorine atoms causes extensive aggregation of fluorinated segments in aqueous solution and hence attenuates the ^{19}F MR signal when the fluoropolymers possess a high density of ^{19}F nuclei.[10] Accordingly, the fluorine content of most reported fluoropolymers is limited to low levels (normally below 5 wt%) in order to maintain sufficient water solubility. Such low fluorine contents are below the levels required for effective ^{19}F MRI studies.

In this report we describe a new class of water-soluble and biocompatible fluoropolymer with high fluorine contents of up to 25 wt%, which are hence highly sensitive for visualization of polymer conjugates by ^{19}F MRI. The fluoropolymers can be readily obtained by polymerizing a carefully-designed fluorinated monomer (Scheme 1a). Despite having a high fluorine content, the fluoropolymers demonstrate high water solubility and outstanding NMR/MRI properties. *In vitro* and *in vivo* imaging studies confirmed that the fluoropolymers provide an intense ^{19}F MRI signal and can thus be used as ^{19}F MRI tracers for visualization of polymer conjugates. To demonstrate the utility of the fluoropolymers for bioconjugation and *in vivo* tracking, we synthesized a protein-polymer conjugate via a graft-from polymerization method using bovine serum albumin (BSA) as a

[a] Dr. C. Fu, X. Tan, Y. Yu, Dr. J. Zhao, Dr C. Zhang, Dr. H. Peng, Prof. A. Whittaker
ARC Centre of Excellence in Convergent Bio-Nano Science and Technology and Australian Institute for Bioengineering and Nanotechnology, The University of Queensland, St Lucia, Queensland, 4072, Australia
E-mail: a.whittaker@uq.edu.au
[b] Dr. B. Demir, Prof. D. Searles
School of Chemistry and Molecular Biosciences and Australian Institute for Bioengineering and Nanotechnology, The University of Queensland, Brisbane, Queensland 4072, Australia
[c] Ms S. Alcantara, Ms H. Kelly, Prof. S. Kent
ARC Centre of Excellence in Convergent Bio-Nano Science and Technology and Department of Microbiology and Immunology, Peter Doherty Institute for Infection and Immunity, The University of Melbourne, Parkville, Victoria 3010, Australia
[d] Dr. V. Kumar, Dr. F. Han, Mr W. Xu, Prof. T. Woodruff
School of Biomedical Sciences, The University of Queensland, St. Lucia, Queensland 4072, Australia
(e) Prof. C. Boyer
Centre for Advanced Macromolecular Design (CAMD) and Australian Centre for NanoMedicine (ACN), School of Chemical Engineering, UNSW Australia, Sydney, NSW 2052, Australia

Supporting information for this article is given via a link at the end of the document.

10.1002/ange.201914119

WILEY-VCH

model therapeutic (Scheme 1b). The BSA-fluoropolymer conjugate displays much improved pharmacokinetic profiles compared with unmodified BSA. Moreover, the presence of the abundant NMR-active ^{19}F nuclei enables non-invasive tracking of the protein conjugate *in vivo* by ^{19}F MRI, providing a means to quantitatively measure a variety of important parameters including rates of clearance and tissue biodistribution of the protein conjugate. We believe that these new fluoropolymers imparting excellent MRI capability to protein conjugates while at the same time extending the blood circulation time of conjugated proteins represent an important alternative to current low-fouling polymers for bioconjugation. Furthermore, the properties of the fluoropolymers lend themselves to numerous other applications in nanomedicine, including in extended lifetime imaging agents, drug delivery vehicles and theranostic agents.

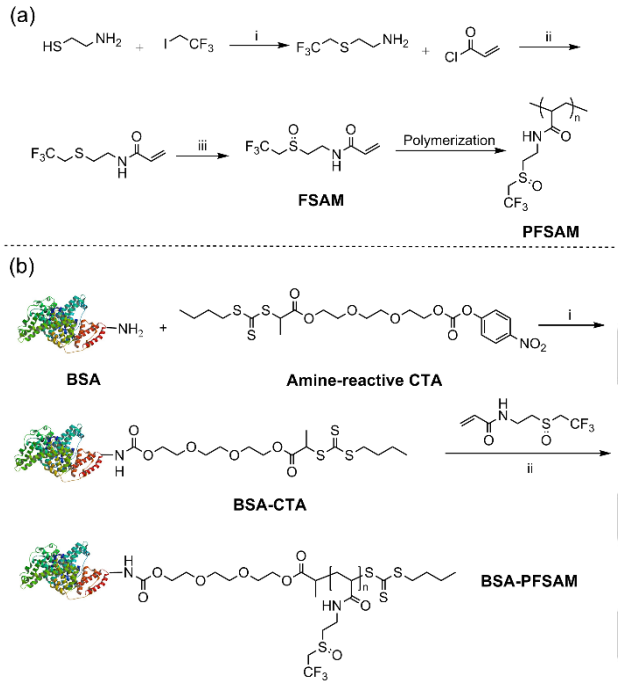

Scheme 1. (a) Synthesis and polymerization of the water-soluble fluorinated monomer FSAM. i) NaOH, DMF, RT, 24 h, 90%; ii) N(Et)$_3$, THF, RT, 24 h, 81%; iii) H_2O_2, acetone, 40 °C, 48 h, 83%. (b) Synthesis of BSA-CTA and BSA-PFSAM conjugate by aqueous controlled photopolymerization. i) PBS, RT, 48 h; ii) Eosin Y, PMDETA, PBS, blue light, RT, 16 h.

Results and Discussion

To ensure sufficient MRI sensitivity for intended biological applications, the fluoropolymers should carry as many fluorine atoms as possible while maintaining good solubility in water. However, the limited range of suitable fluorinated monomers makes this challenging. Current commercially-available fluorinated monomers are invariably highly hydrophobic, and require copolymerization with hydrophilic comonomers to promote water solubility. The introduction of comonomers compromises the overall fluorine content and typically leads to variations in monomer composition and sequence in the resultant fluoropolymers. In order to address this, a new fluorinated monomer N-(2-((2,2,2-trifluoroethyl)sulfinyl)ethyl)acrylamide (FSAM) is proposed in this work and synthesized via three consecutive reactions with an acceptable overall yield of ~ 60% (Scheme 1a). The introduction of polar sulfoxide and amide groups significantly enhances the solubility of FSAM in water, making FSAM a rare non-ionic water-soluble fluorinated monomer containing a high fluorine content of ~ 25 wt%. The new monomer was characterized in detail by ^{1}H, ^{13}C, ^{19}F NMR and 2D NMR spectroscopy (SI, Figures S1-S5).

To investigate the properties of the new polymers, two fluoropolymers (denoted as FP1 and FP2) with target degrees of polymerization (DP) of 50 and 200 were prepared via reversible addition-fragmentation chain transfer (RAFT) polymerization (Figure 1a). High monomer conversion and good control over molecular weight were achieved (Figure 1e). ^{1}H NMR, ^{19}F NMR and size exclusion chromatography (SEC) were used to confirm the successful synthesis of the fluoropolymers (SI, Figures S6-S10). The cytotoxicity of the fluoropolymers was subsequently evaluated by measuring the viability of cells after incubation in the presence of solutions of the fluoropolymers having varied concentrations for 24 h. Both CHO and MDA-MB-468 cells were used for the cytotoxicity studies. The results showed that the fluoropolymers displayed no significant cytotoxicity even at high polymer concentrations of up to 5 mg/mL (SI, Figures S11-S12).

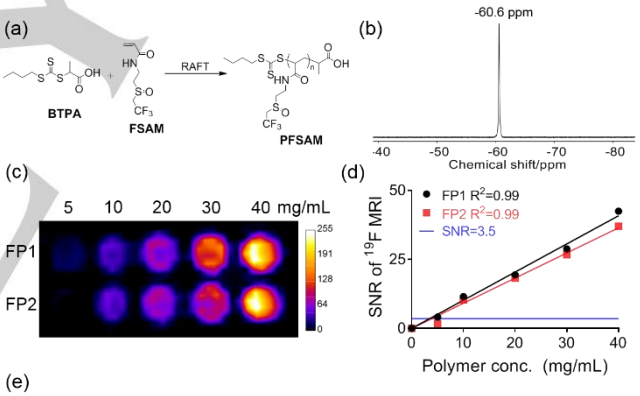

(e)

Polymer	DP	Conv. (%)	$M_{n,NMR}$ (g/mol)	$M_{n,SEC}$ (g/mol)	D_M	T_1 (ms)	T_2 (ms)
FP1	50	95	10540	41570	1.21	909	431
FP2	200	85	35960	72020	1.35	883	373

Figure 1. (a) Synthesis of fluoropolymers PFSAM via RAFT polymerization; (b) ^{19}F NMR spectrum (D_2O) of FP1 (5 mg/mL); (c) ^{19}F MR images of phantom of solutions of FP1 and FP2 at different concentrations; (d) Linear relationship between SNR of ^{19}F MRI and concentration of the fluoropolymers; (e) Properties, including monomer to polymer conversion, molecular weight, dispersity and ^{19}F NMR relaxation times of the fluoropolymers FP1 and FP2.

The aqueous solution properties of the fluoropolymers were subsequently investigated. Both fluoropolymers were readily dissolved in water and displayed an intense single peak at -60.6 ppm in the ^{19}F NMR spectrum (Figure 1b & SI, Figure S13). The ^{19}F NMR relaxation times of the ^{19}F MRI contrast agents (spin-lattice relaxation (T_1) and spin-spin relaxation (T_2) times) are known to be important for determining MRI sensitivity. In general, a short T_1 and a long T_2 relaxation times are required for achieving high MRI sensitivity. Therefore, the T_1 and T_2 relaxation times of

10.1002/ange.201914119

the fluoropolymers were measured using the inversion-recovery and Carr-Purcell-Meiboom-Gill (CPMG) pulse sequences, respectively (Figure 1e). Of particularly note are the long T_2 relaxation times (> 350 ms) of both polymers. Such long T_2 relaxation times are not typically observed for aqueous-dispersed fluoropolymers due to aggregation of fluorinated groups in polymers with high fluorine content. The aggregation of the fluorine-19 nuclei leads to enhanced dipolar coupling with the near-neighbor spins which in turn enhances transverse relaxation (leading to a short T_2). The T_1 relaxation times of the fluoropolymers are comparable to those of previously-reported fluoropolymers. These relaxation times and especially the long T_2 relaxation times, in combination with the high fluorine content, suggest that these fluoropolymers should provide intense ^{19}F MR images with high signal-to-noise ratio (SNR). Therefore, ^{19}F MRI of a series of phantoms of solutions of the fluoropolymers at different concentrations was performed. As shown in Figure 1c, both fluoropolymers can be clearly imaged after a short acquisition time of ~ 13 minutes. A linear relationship between the SNR of the ^{19}F MR images and the concentration of the fluoropolymers in solution was obtained (Figure 1d). This linear relationship indicates no change in the aggregation state of the polymer over this concentration range. If we reasonably propose a minimum SNR of 3.5 for reliable and unequivocal detection of the MRI signal, the detection limit for FP1 was estimated to be 3.4 mg/mL, equating to a detection threshold of approximately 5.28 $\times 10^{17}$ ^{19}F spins per imaging voxel. FP2 also displayed high MRI sensitivity with a similar detection threshold of approximately 5.48 $\times 10^{17}$ ^{19}F spins per voxel despite having a larger molecular weight. Note that these values will be dependent on MRI parameters such as magnetic field strength and configuration of the receiver coil. The short acquisition time used in these experiments, the low detection threshold and the high MRI intensity suggest remarkable imaging sensitivity for both polymers.

The effect of changing temperature on the solution properties of the fluoropolymers was also investigated. Remarkably, aqueous solutions of these fluoropolymers showed pronounced molecular weight-dependent thermo-responsive behavior. In water, FP1 displayed a cloud point (T_{cp}) at ~ 32 °C while FP2 having a larger molecular weight showed a T_{cp} at ~ 26 °C (Figure 2a). The hydrodynamic size of both polymers increased significantly from several nanometers at 25 °C to approximately 1 micrometer at 40 °C (SI, Figures S14-S15), indicative of aggregation of the polymers at the higher temperature. Meanwhile, the single peaks in the ^{19}F NMR spectrum became progressively broader with increasing temperature (Figure 2b & SI, Figure S16). It is notable that the integrated ^{19}F NMR peak intensity of solutions of both polymers was only slightly decreased (< 6%) compared with that at 25 °C (Figure 2c & SI, Figure S17). This is despite both polymers passing through the cloud point below 40 °C and forming larger, aggregated structures. In addition, the ^{1}H NMR signals corresponding to the polymer structures were not attenuated significantly especially for FP1 at temperatures above T_{cp} (SI, Figure S18-S19). Both polymers maintained a relatively long ^{19}F NMR T_2 time (> 289 ms for FP1; > 166 ms for FP2) at 40 °C (Figure 2d & SI, Figure S20). These results suggest that the polymers maintained a high degree of local segmental mobility above the cloud point and hence are likely not strongly dehydrated at the elevated temperatures. This is in sharp contrast to the behavior of previously-examined fluoropolymers, for which dramatic decreases in ^{19}F T_2 and ^{19}F NMR signal intensity were observed when they formed aggregates.[10]

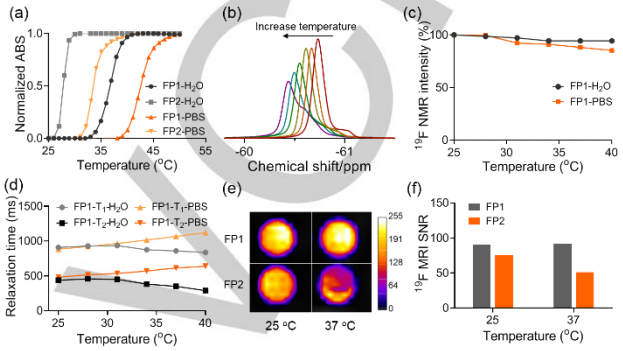

Figure 2. (a) Light absorbance versus temperature for FP1 and FP2 at 5.0 mg/mL in water and PBS measured by UV-Vis; (b) ^{19}F NMR spectra of FP1 in water at different temperatures; (c) ^{19}F NMR intensity of FP1 in water at different temperatures; (d) Relaxation times of FP1 in water and PBS at different temperatures; (e) ^{19}F MRI phantom images and (f) SNR of solutions of FP1 and FP2 in PBS (20 mg/mL) at 25 °C and 37 °C.

The cloud point T_{cp} of FP1 and FP2 in PBS solution was found to increase to 31 °C and 38 °C, respectively (Figure 2a). However, in contrast to solutions in pure water, the relaxation times of FP1 and FP2 increased with increasing temperature in PBS solution (Figure 2d & SI, Figure S20). This is attributed to a "salting-in" effect as a result of the interaction of the PBS salts with the polymer chain segments.[11] The effect of temperature on the MRI of the polymers in PBS was also examined at 25 °C and 37 °C. As shown in Figure 2e and 2f, homogeneous ^{19}F MR images of FP1 was obtained at both temperature while a slightly more intense ^{19}F MRI signal was observed at 37 °C due to enhanced chain mobility at that temperature. In contrast, the inhomogeneous ^{19}F MR image of FP2 at 37 °C was due to aggregation of FP2 and settling of the aggregates at the bottom of the phantom tube (Figure 2e). A decrease in ^{19}F MRI signal intensity was observed for FP2 at 37 °C compared to that at 25 °C (Figure 2f). However, overall strong ^{19}F MRI signals were still observed even for FP2 in the aggregated state, suggesting good chain mobility was maintained, consistent with the results of the NMR studies.

To further understand the solution behavior and its structural basis, molecular dynamics (MD) simulations were performed at temperatures of 20, 50, 80 °C using a system containing three polymers (DP = 10). Due to the short chain length considered, the individual polymer chains did not display a coil-to-globule transition, and as a consequence the radius of gyration (R_g) of the chains remained constant with temperature increasing from 20 to 80 °C (SI, Figure S21). However, at the higher temperature (80 °C), intermolecular aggregation through the backbone of the

10.1002/ange.201914119

polymers was apparent, evidenced by closer mutual distances of the three polymers compared to 20 and 50 °C (SI, Figure S22). The radial distribution functions (RDF) between the atomic center/center-of-mass of different structures of the polymers including the sulfoxide (S=O), amide (CONH), trifluoromethyl (CF_3) and backbone ($CHCH_2$) units with water molecules as a function of temperature were calculated to investigate the extent of hydration and solvent structure around the polymers (SI, Figure S23). The results revealed that the dehydration of the backbone structure of the polymers upon temperature increasing was much more significant compared to other structures, leading to intermolecular aggregation through the backbone interactions at higher temperature (SI, Figure S22d & Table S1). Of relevance to this study, the introduction of highly hydrophilic sulfoxide group adjacent to the CF_3 group results in minimal dehydration of the CF_3 groups on an increase in temperature, and so these groups remain sufficiently hydrated and maintain high mobility at higher temperatures. This accounts for the retention of favorable NMR properties such as a long T_2 relaxation time and outstanding ^{19}F MRI performance of the polymers in the aggregated state.

Many MRI contrast agents are administered via intravenous injection and will rapidly encounter in the primary defense a variety of circulating cells especially phagocytic and non-phagocytic white blood cells (WBCs) responsible for protecting the body against foreign invaders. The association of the fluoropolymers with such cells could significantly influence their circulation behavior as well as eventual accumulation in various tissues. To investigate this, we incubated FP1 and FP2 labeled with fluorescein dye in fresh human blood at a concentration of 100 µg/mL at 37 °C and examined their association with six different WBC populations.[12] Overall, the fluoropolymers showed low levels of association with the WBCs (< 5% association) in the whole blood assay while the fluoropolymer FP2, which forms aggregates at the investigated temperature, showed an enhanced association (~ 13.5%) with B cells, a non-phagocytic lymphocyte (Figure 3a). This effect is likely mediated by interaction with complement proteins in the plasma and binding to abundant complement receptors on the B cells. To confirm the influence of plasma proteins binding to the materials and so influencing interactions with WBCs, we studied association of the polymers with WBCs in washed blood devoid of plasma proteins. We found that the association of FP1 and FP2 with all the WBC populations including monocytes and B cells was largely attenuated (Figure 3b). These results suggest strongly that the observed association of FP1 and FP2 with the WBC populations is facilitated by their interaction with certain plasma proteins in the blood. However, overall, these fluoropolymers interact weakly with human blood WBC populations.

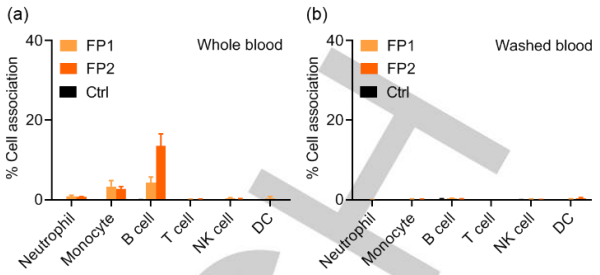

Figure 3. Association of human fresh white blood cells with the polymers tested in (a) whole human blood and (b) washed blood without plasma proteins at 37 °C. The control group was cells treated with PBS. Six different WBC populations were identified and assessed for association with the fluorescent materials by flow cytometry.

The suitability of the fluoropolymers as ^{19}F MRI contrast agents was tested using a healthy murine model. In each experiment, a solution of the fluoropolymers in PBS buffer (containing ~ 0.1 mmol ^{19}F) was injected into the mice via the lateral tail vein. The mice were immediately placed in a 9.4 T MRI scanner and ^{1}H (for anatomical registration) and ^{19}F MR images collected. The acquisition time for each ^{19}F MRI scan was 17 minutes, and the ^{19}F MR images were overlaid with corresponding ^{1}H MR images. As shown in Figure 4a, intense ^{19}F MRI signals could be clearly observed for the mice injected with the fluoropolymers, suggesting outstanding *in vivo* MRI sensitivity. The clearance pathway of the polymers was found to be strongly dependent on their size. FP1, with a smaller size (~ 4.3 nm in PBS at 37 °C, Figure S14), underwent rapid renal clearance and the ^{19}F signal was observed primarily in the kidneys and bladder (Figure 4a). At 24 h post-injection, no ^{19}F MR signal of FP1 was observed. In contrast, FP2 which forms larger aggregates at body temperature (~ 836 nm in PBS, Figure S15) accumulated largely in the liver and underwent much slower clearance. Strong ^{19}F MRI signals were still present in the mice at 24 h post-injection (Figure 4a). This is consistent with previous reports that large particles demonstrate high and long-term accumulation in organs such as the liver with much slower clearance compared with small molecules/particles.[13] At two months after injection, the organs of the mice were harvested and subjected to histological examination. The histological results showed no tissue damage, indicative of excellent biocompatibility of the fluoropolymers (Figure 4b).

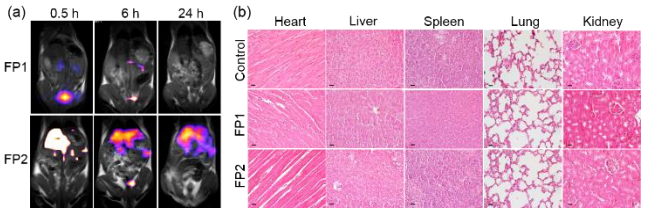

Figure 4. (a) Superimposed ^{1}H and ^{19}F MR images of mice after injection with solutions of FP1 or FP2, recorded at different times post injection; (b) Histological examination of different organs (H&E staining, 40 ×) collected from mice at two months after injection of the polymer solutions. The control group was mice treated with PBS. Scale bar: 20 µm.

10.1002/ange.201914119

WILEY-VCH

RESEARCH ARTICLE

The weak interaction with the WBCs and the intense ^{19}F MRI signal of the fluoropolymers underlines their potential for attachment to biomolecules for extending pharmacokinetics and tracking the location of the biomolecules through MRI. Accordingly we prepared a protein-fluoropolymer conjugate using BSA as the model protein via a graft-from method by photoinduced electron/energy transfer-RAFT (PET-RAFT) polymerization (Scheme 1b). [14, 15] Details of the characterizations of the BSA macro CTA (BSA-CTA) and PET-RAFT polymerization can be found in the Supporting Information (SI, Figure S24-S26). The successful grafting of PFSAM polymers to BSA was confirmed by ^{1}H NMR, ^{19}F NMR and SDS-PAGE (Figure 5a-c). ^{19}F MRI of a phantom of a solution of BSA-PFSAM conjugate (Figure 5d) shows that a strong MRI signal is maintained in the conjugate. The ^{19}F NMR relaxation times of the conjugate, T_1 and T_2, were measured to be 846 and 195 ms, respectively. The long T_2 relaxation time of the conjugate shows that despite being grafted onto the BSA, the fluoropolymers maintained high segmental mobility necessary for effective ^{19}F MR imaging. The properties of the conjugate as a function of temperature were investigated by DLS. The mean size of the conjugate increased from ~ 20 nm to 32 nm with temperature increasing from 25 °C to 40 °C (SI, Figure S27). Finally, the esterase-like activity of the conjugate was evaluated by measurement of the rate of hydrolysis of 4-nitrophenyl acetate,[14] and the results showed that the conjugate suffered no loss of the activity as compared with native BSA (SI, Figure S28).

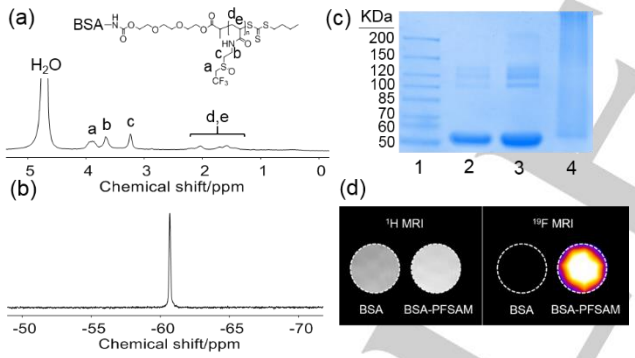

Figure 5. (a) ^{1}H NMR and (b) ^{19}F NMR spectra (D_2O) of BSA-PFSAM conjugate; (c) SDS-PAGE of protein marker (lane 1), BSA (lane 2), BSA-CTA (lane 3) and BSA-PFSAM conjugate (lane 4); (d) ^{1}H/^{19}F MRI of solutions of BSA and BSA-PFSAM conjugate (20 mg/mL).

The *in vivo* pharmacokinetics and biodistribution of the protein-fluoropolymer conjugate were next examined. A PEGylated BSA conjugate BSA-PEG was also prepared for comparison studies by the PET-RAFT polymerization of oligo(ethylene glycol) monomethyl ether acrylate (PEGA, M_w=480) using the BSA-CTA (SI, Figure S29). To enable the study of pharmacokinetics and biodistribution, BSA and the BSA conjugates were covalently labelled with a NIR dye Cy7.5 and injected intravenously into the mice via the tail vein. Figure 6a shows the concentration of BSA and BSA-polymer conjugates in the blood over time after injection. The pharmacokinetic parameters for BSA and the conjugates were calculated by fitting the data using a three-compartment model and the results are summarized in Table S2. It can be seen that all three samples were rapidly distributed with similar half-life in the alpha phase ($t_{1/2,\alpha}$) ranging from 0.30 h to 0.44 h. After the rapid distribution, the samples underwent a biphasic elimination process. Both BSA-PFSAM and BSA-PEG displayed a longer elimination half-life at the beta phase ($t_{1/2,\beta}$) and gamma phase ($t_{1/2,\gamma}$) than BSA. In particular, the BSA-PFSAM conjugate showed a $t_{1/2,\beta}$ of 11.13 h compared to the BSA-PEG conjugate ($t_{1/2,\beta}$ = 15.47 h), and was ~ 3-fold longer than that of BSA ($t_{1/2,\beta}$ = 3.90 h).

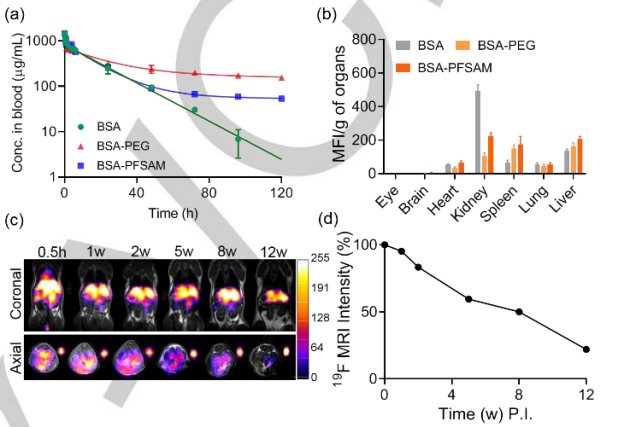

Figure 6. (a) Pharmacokinetics of BSA, BSA-PEG and BSA-PFSAM; (b) Biodistribution of BSA, BSA-PEG and BSA-PFSAM at 5 days post-injection; (c) Time-dependent coronal and axial ^{19}F/^{1}H MR images of mice after injection of BSA-PFSAM; (d) ^{19}F MRI signal intensity of the mice relative to a solution of FSAM (2 mg/mL in water).

Further analysis of the terminal blood samples revealed the BSA-PFSAM conjugate presented a lower blood to plasma ratio than BSA and the BSA-PEG conjugate (SI, Figure S30), suggesting that BSA-PFSAM exhibited lower binding to cellular components of blood than BSA and BSA-PEG. The whole-body biodistribution of BSA and the BSA conjugates was further investigated by measurement of the fluorescence of excised organs (Figure 6b), and revealed that the biomolecules accumulated in the major organs except the eye and brain. Compared with the conjugates, BSA showed the highest mean fluorescence intensity (MFI)/g in the kidneys, suggesting a more rapid renal excretion, as is expected for the smaller molecule. Both conjugates underwent slower renal clearance compared with BSA and accumulated in organs such as the liver, kidneys and spleen. Collectively, these results indicate that the conjugation of the fluoropolymer PFSAM to a model protein BSA can effectively prolong the circulation time of the protein in the bloodstream in a manner similar to PEGylation.

The results to this point demonstrate that conjugation with the water-soluble fluoropolymer can extend the pharmacokinetics of the model protein. The high density of fluorine atoms on the hydrophilic chains provides the potential for tracking the protein conjugates *in vivo* by ^{19}F MRI. Such a possibility will allow non-invasive and real-time monitoring of the biodistribution and clearance of protein and other biomolecule conjugates. To test whether this can be realized, a solution of BSA-PFSAM conjugate (containing ~ 0.053 mmol ^{19}F) was injected into mice and

monitored by ^{19}F MRI at different time points after injection. The MRI scan time was ~ 17 minutes. As shown in Figure 6c, intense ^{19}F MRI signals were observed in the major organs of the mice, highlighting the outstanding imaging sensitivity of the conjugate. It can be seen that the majority of the conjugate accumulated within the liver. The presence of the conjugate in the organs was also confirmed by ^{19}F NMR of tissue homogenates (SI, Figure S31). With increasing time the conjugate was slowly cleared from the body as reflected by the progressive decrease in the ^{19}F MRI signals. By comparing the ^{19}F MRI signal intensity to that of a reference solution of FSAM, the rate of *in vivo* clearance of the conjugate could be quantified (Figure 6d). The gradual clearance of the conjugate was also verified by the observed decrease in the signal intensity of whole-body ^{19}F NMR of the mice (SI, Figure S32).

Conclusion

In conclusion, we have introduced a new class of water-soluble fluoropolymer with potential broad applications for bioconjugation. The incorporation of the highly hydrophilic sulfoxide group in the fluorinated acrylamide-based monomer endows the fluoropolymers with excellent water solubility despite the high fluorine content. The fluoropolymers showed interesting solution properties and more importantly demonstrated outstanding imaging sensitivity as ^{19}F MRI contrast agents, which opens up new possibilities for further *in vivo* applications. Using BSA as a model therapeutic molecule, we successfully synthesized a protein-fluoropolymer conjugate via a graft-from method mediated by a photopolymerization technology. Due to the mild conjugation conditions, the conjugate maintained good esterase activity. Moreover, the NMR/MRI properties of the conjugate are suitable for *in vivo* ^{19}F MRI applications. Pharmacokinetic studies showed that conjugation of the fluoropolymers can significantly prolong the circulation time of BSA in the bloodstream. Further MRI studies revealed that the conjugate could be clearly observed under ^{19}F MRI with outstanding sensitivity, allowing information including the biodistribution and clearance profile of the protein-polymer conjugate to be examined quantitatively. The capacity to obtain such information in real-time without additional conjugation of imaging moieties highlights the benefits of using fluoropolymers for protein conjugation over other polymers. Therefore, we believe that the fluoropolymers developed in this work will be an important complement to current approaches to bioconjugation, allowing the synthesis of the next generation of self-trackable therapeutic polymer conjugates.

Acknowledgements

A.W. acknowledges the financial support from Australian Research Council (CE140100036, DP0987407, DFP110104299, DFP180101221, LE0775684, LE0668517, and LE0882357) and the National Health and Medical Research Council (APFP1021759). C.F. acknowledges the University of Queensland for a UQ Development Fellowship (UQFEL1831361). T.M.W acknowledges support from the National Health and Medical Research Council (APP1118881 and APP1105420). B.D. and D.J.S acknowledge support from the Queensland Cyber Infrastructure Foundation (QCIF) and the University of Queensland Research Computing Centre. The Australian National Fabrication Facility, Queensland Node, is also acknowledged for access to some items of equipment.

Keywords: Bioconjugation • ^{19}F MRI • In vivo tracking • Low-fouling fluoropolymers • Thermo-responsive materials

[1] a) J. S. Suk, Q. Xu, N. Kim, J. Hanes, L. M. Ensign, *Adv. Drug Deliv. Rev.* **2016**, *99*, 28-51; b) S. C. Larnaudie, J. Sanchis, T.-H. Nguyen, R. Peltier, S. Catrouillet, J. C. Brendel, C. J. Porter, K. A. Jolliffe, S. Perrier, *Biomaterials* **2018**, *178*, 570-582; c) Y. Hou, J. Yuan, Y. Zhou, J. Yu, H. Lu, *J. Am. Chem. Soc.* **2016**, *138*, 10995-11000; d) X. Liu, M. Sun, J. Sun, J. Hu, Z. Wang, J. Guo, W. Gao, *J. Am. Chem. Soc.* **2018**, *140*, 10435-10438; e) R. J. Mancini, J. Lee, H. D. Maynard, *J. Am. Chem. Soc.* **2012**, *134*, 8474-8479; f) N. Adams, U. S. Schubert, *Adv. Drug Deliv. Rev.* **2007**, *59*, 1504-1520; g) A. J. Keefe, S. Jiang, *Nat. Chem.* **2012**, *4*, 59; h) F. Wurm, C. Dingels, H. Frey, H.-A. Klok, *Biomacromolecules* **2012**, *13*, 1161-1171; i) L. Tao, G. Mantovani, F. Lecolley, D. M. Haddleton, *J. Am. Chem. Soc.* **2004**, *126*, 13220-13221; j) A. J. Keefe, S. Jiang, *Nat.Chem.* **2012**, *4*, 59.

[2] J. Nicolas, V. San Miguel, G. Mantovani, D. M. Haddleton, *Chem. Comm.* **2006**, 4697-4699.

[3] L. S. Karfeld-Sulzer, E. A. Waters, N. E. Davis, T. J. Meade, A. E. Barron, *Biomacromolecules* **2010**, *11*, 1429-1436.

[4] Q. Li, J. B. White, N. C. Peterson, K. W. Rickert, C. O. Lloyd, K. L. Allen, K. Rosenthal, X. Gao, H. Wu, W. F. Dall'Acqua, *J. Control. Release* **2018**, *279*, 126-135.

[5] a) T.-L. Cheng, K.-H. Chuang, B.-M. Chen, S. R. Roffler, *Bioconjugate Chem.* **2012**, *23*, 881-899; b) P. Debie, J. Van Quathem, I. Hansen, G. Bala, S. Massa, N. Devoogdt, C. Xavier, S. Hernot, *Mol. Pharm.* **2017**, *14*, 1145-1153; c) C. Cilliers, I. Nessler, N. Christodolu, G. M. Thurber, *Mol. Pharm.* **2017**, *14*, 1623-1633.

[6] a) M. A. Sowers, J. R. McCombs, Y. Wang, J. T. Paletta, S. W. Morton, E. C. Dreaden, M. D. Boska, M. F. Ottaviani, P. T. Hammond, A. Rajca, *Nat. Commun.* **2014**, *5*, 5460; b) H. Yamada, Y. Hasegawa, H. Imai, Y. Takayama, F. Sugihara, T. Matsuda, H. Tochio, M. Shirakawa, S. Sando, Y. Kimura, *J. Am. Chem. Soc.* **2015**, *137*, 799-806.

[7] I. Tirotta, V. Dichiarante, C. Pigliacelli, G. Cavallo, G. Terraneo, F. B. Bombelli, P. Metrangolo, G. Resnati, *Chem. Rev.* **2014**, *115*, 1106-1129.

[8] a) Z. X. Jiang, X. Liu, E. K. Jeong, Y. B. Yu, *Angew. Chem. Int. Ed.* **2009**, *48*, 4755-4758; b) I. Tirotta, A. Mastropietro, C. Cordiglieri, L. Gazzera, F. Baggi, G. Baselli, M. G. Bruzzone, I. Zucca, G. Cavallo, G. Terraneo, *J. Am. Chem. Soc.* **2014**, *136*, 8524-8527; c) O. Munkhbat, M. Canakci, S. Zheng, W. Hu, B. Osborne, A. A. Bogdanov, S. Thayumanavan, *Biomacromolecules* **2018**, *20*, 790-800; d) A. A. Kislukhin, H. Xu, S. R. Adams, K. H. Narsinh, R. Y. Tsien, E. T. Ahrens, *Nat. Mater.* **2016**, *15*, 662; e) A. T. Preslar, F. Tantakitti, K. Park, S. Zhang, S. I. Stupp, T. J. Meade, *ACS nano* **2016**, *10*, 7376-7384.

[9] a) K. J. Thurecht, I. Blakey, H. Peng, O. Squires, S. Hsu, C. Alexander, A. K. Whittaker, *J. Am. Chem. Soc.* **2010**, *132*, 5336-5337; b) C. Zhang, S. S. Moonshi, W. Wang, H. T. Ta, Y. Han, F. Y. Han, H. Peng, P. Král, B. E. Rolfe, J. J. Gooding, *ACS nano* **2018**, *12*, 9162-9176.

[10] a) H. Peng, I. Blakey, B. Dargaville, F. Rasoul, S. Rose, A. K. Whittaker, *Biomacromolecules* **2009**, *10*, 374-381; b) C. Fu, C. Zhang, H. Peng, F. Han, C. Baker, Y. Wu, H. Ta, A. K. Whittaker, *Macromolecules* **2018**, *51*, 5875-5882; c) Y. Koda, T. Terashima, M. Sawamoto, H. D. Maynard, *Polym. Chem.* **2015**, *6*, 240-247.

[11] R. Bhat, H. Patel, P.-C. Tsai, X.-L. Sun, D. Daoud, R. Lalancette, B. Michniak-Kohn, A. Pietrangelo, *Polym. Chem.* **2015**, *6*, 5993-6000.

10.1002/ange.201914119

[12] a) J. J. Glass, L. Chen, S. Alcantara, E. J. Crampin, K. J. Thurecht, R. De Rose, S. J. Kent, *ACS Macro Lett.* **2017**, *6*, 586-592; b) J. J. Glass, Y. Li, R. De Rose, A. P. Johnston, E. I. Czuba, S. Y. Khor, J. F. Quinn, M. R. Whittaker, T. P. Davis, S. J. Kent, *ACS Appl. Mater. Interfaces* **2017**, *9*, 12182-12194.

[13] a) J. Huang, L. Bu, J. Xie, K. Chen, Z. Cheng, X. Li, X. Chen, *ACS nano* **2010**, *4*, 7151-7160; b) C. He, Y. Hu, L. Yin, C. Tang, C. Yin, *Biomaterials* **2010**, *31*, 3657-3666.

[14] J. Xu, K. Jung, N. A. Corrigan, C. Boyer, *Chem. Sci.* **2014**, *5*, 3568-3575.

[15] B. S. Tucker, M. L. Coughlin, C. A. Figg, B. S. Sumerlin, *ACS Macro Lett.* **2017**, *6*, 452-457.

10.1002/ange.201914119

WILEY-VCH

Entry for the Table of Contents (Please choose one layout)

RESEARCH ARTICLE

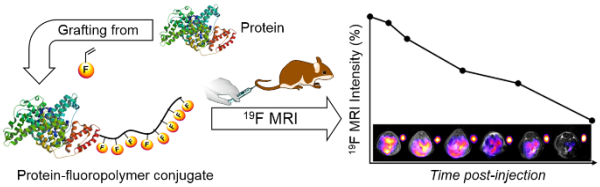

*Changkui Fu, Baris Demir, Sheilajen Alcantara, Vinod Kumar, Felicity Han, Hannah G. Kelly, Xiao Tan, Ye Yu, Weizhi Xu, Jiacheng Zhao, Cheng Zhang, Hui Peng, Cyrille Boyer, Trent M. Woodruff, Stephen J. Kent, Debra J. Searles, Andrew K. Whittaker**

Page No. – Page No.

Low-fouling Fluoropolymers for Bioconjugation and In Vivo Tracking

Water-souble low-fouling fluoropolymers with high fluorine content demonstrate outstanding ^{19}F magnetic resonance imaging sensitivity and have been used as self-trackable polymers for bioconjugation and *in vivo* tracking.